$U\text{-}O_{yl}$ stretching vibrations as a quantitative measure of equatorial bond covalency in uranyl complexes: a quantum chemical investigation

Poppy Di Pietro[1] and Andrew Kerridge*[1,2]

[1] *Department of Chemistry, University College London, 20 Gordon Street, London, WC1H 0AJ, UK.*

[2] *Department of Chemistry, Lancaster University, Lancaster, LA1 4YW, UK.*

E-mail: a.kerridge@lancaster.ac.uk

Abstract

The molecular structures of a series of uranyl (UO_2^{2+}) complexes in which the uranium centre is equatorially coordinated by a first row species are calculated at the density functional theoretical (DFT) level and binding energies deduced. The resulting electronic structures are investigated using a variety of density-based analysis techniques in order to quantify the degree of covalency in the equatorial bonds. It is shown that a consideration of properties of both the one-electron and electron-pair densities is required to understand and rationalise the variation in axial bonding effected by equatorial complexation. Strong correlations are found between density-based measures of covalency and equatorial binding energies, implying a stabilising effect due to covalent interaction, and it is proposed that uranyl U-O_{yl} stretching vibrational frequencies can serve as an experimental probe of equatorial covalency.

Introduction

The electronic complexities of f-element compounds, which exhibit pronounced relativistic effects, weak crystal fields and strongly correlated subsystems[1] make the characterisation of bonding a challenging problem to both experimentalists and theorists alike, with different analyses leading to substantial variation in conclusions[2]. Unambiguous characterisation is, however, of both fundamental and practical importance. From a fundamental perspective, a deeper understanding of bonding interactions can, amongst other things, aid in the assessment of the viability of novel synthetic targets, while from a practical perspective, variation in bonding character can be exploited in selective complexation. This is of particular current relevance to the nuclear power industry, where the chemical separation of trivalent actinides and lanthanides provides a potential strategy for the efficient remediation of spent nuclear fuel[3,4]. These separation processes have their foundations in the relative stability of actinide (An) complexes over their lanthanides (Ln) analogues. It is presumed that this stability is derived from an enhanced covalent interaction in the former due to the increased radial extent, and therefore chemical accessibility, of the An 5f over the Ln 4f orbitals. To date, however, a robust correlation between enhanced covalency and enhanced stability remains undemonstrated.

In this contribution, we focus on analyses of the experimentally observable electron density with the aim of relating the variation in U-O_{yl} stretching vibrations and, by implication, the strength of the U-O bonds, to the changes in electronic structure due to equatorial complexation by monodentate ligands. In order to achieve this, we have considered the following ligands: H_2O, OH^-, CO, CN^-, NCS^- and F^-, of which all coordinate uranyl via a first row species and have been chosen as they are expected to provide a range of interaction strengths. Of these, the aquo complex has been experimentally well-characterised in the

aqueous phase by X-ray absorption spectroscopy (XAS)[5,6] as consisting of 5 coordinating water molecules in the equatorial plane of the uranyl unit, whereas the equatorial coordination number reduces to four in the case of the hydroxide complex[6]. Of the pseudohalides considered here, $[UO_2(NCS)_5]^{3-}$ is formed in 15M sodium thiocyanate solution and has been characterised in the solid-state[7], with Raman spectroscopy providing evidence of thiocyanate complexation in the aqueous phase, whereas $[UO_2(CN)_5]^{3-}$ is formed in the reaction of $UO_2(OTf)_2$ with NEt_4CN in acetonitrile[8]. When considering the fluoride, extended X-ray absorption fine structure (EXAFS) data obtained in 3M $N(CH_3)_4F$ solution[9] gives an F coordination number of 4.4 ± 0.6, with density functional theory (DFT) simulations finding $UO_2F_5^{3-}$ to be stable in an aqueous environment[9,10]. DFT simulations also confirm the 5-coordinate nature of the aquo complex[11–14] along with the reduction in coordination in more basic environments[6,9,13,15]. Cyano and isocyano uranyl complexes have also been studied theoretically[15–17], where a preference for binding through the carbon atom was found.

Previous calculations have found a weakening of the U-O interaction in similar complexes[18] and this was attributed, via molecular orbital analyses, as being due to π or σ donation, where ligands compete with the uranyl oxygen ions for the U 5f, 6p or 6d orbitals, acting to weaken the covalent interaction. This is, however, in contrast to the findings of Ingram *et al.*, who attribute the weakening to a reduction in the $U\text{-}O_{yl}$ *ionic* interaction[13]. This apparent contradiction provides a motivation for the use of density based, rather than orbital based, analyses.

Here, we present results of DFT simulations on these uranyl complexes and combine a series of state of the art density-based analysis techniques in order to detail the relationship between equatorial bond covalency and the variation in experimentally observable properties of the

axial U-O_{yl} bond. We find several strong correlations that support a relationship between equatorial bond covalency and energetic stability and demonstrate that uranyl vibrational modes act as a sensitive probe of this covalent character. We also analyse the electronic effects of equatorial coordination in unprecedented detail.

Computational details

All calculations were performed at the density functional theoretical (DFT) level using Version 6.4 of the TURBOMOLE quantum chemistry package[19]. For geometry optimisations and vibrational frequency analysis, Ahlrichs basis sets of polarized triple-zeta quality[20] (def-TZVP for U and def2-TZVP for all other atoms) were used used along with an associated relativistically contracted effective core potential which replaced 60 core electrons on the uranium centre[21]. Subsequent single-point calculations performed on the optimised structures employed the segmented all-electron relativistically contracted (SARC) basis set[22] on the U centre, with scalar relativistic effects modelled using the 2nd order Douglas-Kroll-Hess Hamiltonian[23,24]. Due to the closed shell nature of these systems, the effects of spin-orbit coupling were not included in the calculations. Two exchange-correlation (XC-) functionals were chosen for this study: the non-empirical meta-GGA TPPS functional[25] and the related hybrid functional, TPSSh[26], the latter containing a 10% contribution of exact exchange. TPSS has proved superior to GGA functionals in its modelling of the electronic structure of hydrated uranyl[27] and bulk actinide oxides[28], as well as producing extremely accurate hydration energies in aquo complexes of other ions[29]. TPPSh was chosen so as to investigate the effect of the inclusion of exact exchange on binding energies and other properties: previous work has reported improved uranyl reaction energies when employing hybrid functionals[27]. The PBE[30] and B3LYP[31,32] functionals were also employed in order to

investigate the robustness of our calculated quantities. In order to stabilise anionic electronic structures, geometries were optimised using default optimisation criteria in the presence of a continuum aqueous solvent, defined using the COSMO model[33] (radii: H = 1.30Å, C = 2.00Å, N = 1.83Å, O = 1.72 Å, F = 1.72Å, S = 2.16Å, U = 2.23Å). Energetic stability was verified by performing numerical frequency analysis (within the harmonic approximation) on the optimised structures. All-electron densities were used as the starting point for further analysis, employing the AIMAll[34] (Version 13.11.04), Multiwfn[35] (Version 3.2) and NBO[36] (version 6.0) codes.

Results and Discussion

We consider a series of ligands bound to the uranium centre via first row species, namely H_2O, OH^-, CO, CN^-, NCS^- and F^-, the aim being to establish the variation in bonding as one traverses the heavier first row elements.

Binding energies as a function of coordination number

The limiting equatorial coordination number of hydroxo complexes has been shown to be four[6,37] whereas the aquo and fluoro complexes have been reported with an equatorial coordination number of five[7,9,37–39]. The monocationic $[UO_2(CO)_5]^+$ complex has also been reported in the gas phase[40]. Several theoretical studies support the experimentally derived coordination numbers of the hydroxo and aquo complexes[6,9,11–13,15,41–43], whereas the data for

the other species considered in this study are less numerous[9,15,44–46]. Bearing this in mind, we employed the TPSS and TPSSh functionals to first investigate the relative stabilities of the fluoro, cyano, isocyano and carbonyl complexes of uranyl when varying the equatorial coordination from four to six. The results of these calculations can be found in Table 1.

Binding energies were calculated as the total energy difference between the complex and the sum of the uranyl and individual ligand fragments. From these total energy differences, relative stabilities as a function of coordination number were deduced. It should be noted that the relative stabilities evaluated here assume excess ligand concentration and are therefore not representative of typical experimental conditions: in the context of this study, they serve only to identify complexes for subsequent analysis.

In agreement with the previous study of Sonnenberg *et al.*[15], we find coordination of uranyl by five cyano/isocyano ligands to be energetically favourable in aqueous solution, with the D_{5h}-symmetry cyano complex more stable than the isocyano by 0.62 eV (0.61 eV) when using the TPSS (TPSSh) functional. In contrast to this previous study, however, we find all carbonyl complexes to be stable in aqueous solution, albeit with binding energies much smaller than the isoelectronic (iso)cyano complexes and also significantly smaller than the binding energy of the aquo complex. Therefore, although coordination by six carbonyl ligands is found to be the energetically favourable complex, in practise these carbonyl ligands would be easily displaced by water. We note that coordination by six cyano ligands is just 0.13 eV less stable at the TPSS level than that by five, with the inclusion of exact exchange leading to a 0.07 eV destabilisation of the higher coordination complex. Finally, we find that five-fold coordination gives a more stable fluoro complex than that with four or six coordinating species, with the latter complex being highly non-planar with substantial distortion of the uranyl unit, indicating significant steric hindrance. Vallet et al.[9] have also found theoretical evidence for the existence of $[UO_2(F)_5]^{3-}$ in solution.

Structural and vibrational characterisation

In Table 2, we report key structural parameters of the energetically most stable complexes considered in the remainder of this study. We find that all XC-functionals are able to accurately reproduce experimentally determined structures, albeit with a small but consistent overestimate of axial U-O_{yl} bond lengths in all but the aquo complex. In this regard, hybrid functionals outperform the pure functionals, with an approximately 40% reduction in the mean average deviation (MAD) of the axial U-O_{yl} bond. When considering the weaker, longer equatorial bonds, all functionals perform excellently, with MADs of less than 0.01 Å for all functionals excluding B3LYP, demonstrating the suitability of our model chemistry to these systems.

It has been established that the uranyl U-O_{yl} stretch vibrations are a sensitive probe of its coordination environment[47–51] and so we investigated the calculated U-O_{yl} vibrational frequencies for the complexes considered here. The frequencies are reported in Table 3. In every case, values calculated using hybrid functionals are higher than those obtained using pure functionals, as expected based on the shorter calculated U- O_{yl} bond lengths discussed above. In order to establish a possible correlation between U- O_{yl} vibrational frequencies and uranyl-ligand bond lengths, linear regression was performed. This regression revealed only relatively weak correlation between these two parameters, with R^2 values ranging from 0.72 to 0.79 depending on the XC-functional and symmetry of the vibration.

We now consider the binding energies of the complexes under investigation here. Binding energies were calculated in the same manner as those reported in Table 1 and are given in Table 4, in order of increasing binding energy per ligand. We sought to establish a correlation between total binding energies and uranyl stretch frequencies and found a strong relationship,

as can be seen in Figure 1. When considering correlation with the antisymmetric stretching mode, linear regression analysis produced R^2 values of 0.97-0.98 for the four functionals, respectively, whereas correlation with the symmetric stretching mode produced R^2 values of 0.90-0.98. Of these, the TPSSh functional gave the highest correlation in both cases. Bearing in mind the accuracy of the molecular structures obtained using the TPSSh functional and the identical trends in binding energies when comparing the two functionals, along with overall similarity in predicted properties, the remainder of this study considers only TPSSh-derived data.

Density-based analyses of electronic structure

We sought to understand the strong correlations between binding energies and U-O_{yl} stretch frequencies in terms of the electron density, i.e. without resorting to analysis of the canonical Kohn-Sham orbitals. In many situations the electronic structure of f-element complexes cannot be well-described using monodeterminantal methods[52–56] and the use of multireference methods such as complete-active-space self-consistent-field (CASSCF) or multireference configurational interaction (MRCI) approaches brings the validity of orbital based analysis methods into question. It is therefore our opinion that methods of analysis that are equally well-suited to monoconfigurational density-based and multireference wavefunction-based approaches are best pursued so as to allow results of these different methodologies to be directly compared. We also note the success of such density-based methods of analysis of f-element complexes in the literature[2,57–61], including some of the systems under consideration here[51].

We begin with a visual inspection. Figure 2 shows the electron density differences upon complexation for the carbonyl, isocyano and fluoro complexes, a representative group

exhibiting weak, intermediate and strong binding (density difference plots for all complexes considered here can be found in ESI). These density differences are obtained by taking the total electron density of the complex and subtracting from this the densities of the separate uranyl and ligand fragments, held fixed at the geometry of the optimised complex. There are two distinct trends that may be identified from these plots: firstly, as one considers more strongly bound complexes, so the blue isosurfaces, corresponding to charge accumulation, become localised in the bonding region between the uranium centre and the equatorial ligand. This may be indicative of a directed interaction with more covalent character. Secondly, the more strongly binding ligands induce a notable redistribution of charge within the uranyl unit. This redistribution corresponds to charge depletion in the U-O_{yl} bonding region, represented by the yellow isosurfaces, indicating a reduction in the covalent character of the U-O_{yl} bond. This is presumably due to the competing interactions in the equatorial plane and leads to the previously discussed weakening of the U-O_{yl} bond, as evidenced by the reduced vibrational frequencies. Along with this reduction in covalent U-O_{yl} bond character is a commensurate accumulation of charge on the oxygen centres, indicated by the blue isosurfaces, indicating enhanced ionic character in the U-O_{yl} bond. Finally, we also note the strong qualitative similarity in the density difference plots of the fluoride and hydroxide complexes, which are also found to have very similar binding energies.

In order to further rationalise the density difference plots we turned to a more quantitative method, QTAIM. QTAIM allows us to consider both topological and integrated properties of the electron density: we first consider the topological characteristics, summarised in Table 5.

Looking first at the values of ρ_{BCP} (the magnitude of the electronic density at the bond critical point, BCP) of the U-O_{yl} bond, we find an almost monotonic decrease as the binding energy of the complex increases, a trend that is mirrored by H (the energy density at the BCP). This might be expected since we have shown in Figure 1 that increased equatorial binding leads to

a weakening and lengthening of the axial U-O_{yl} bond. However, the correlation between the U-O_{yl} ρ_{BCP} and complex binding energy is striking (R^2 = 0.98, see Figure 3(a)), as is the correlation with H (R^2 = 0.98). Specifically, the QTAIM parameters indicate a reduction in covalent character in the U-O_{yl} bond upon complexation, commensurate with the trend seen in Figure 2, which shows that strongly binding equatorial ligands deplete charge density in the axial U-O_{yl} bonding region. When considering the equatorial ligands themselves, correlation between ρ_{BCP} and ligand binding energy is also strong (R^2 = 0.97, see Figure 3(b)). This is somewhat surprising, bearing in mind the range of coordinating species, but demonstrates that variations in bond strength are well accounted for in terms of variation in covalent bonding character. The correlation with H is slightly poorer (R^2 = 0.91), however we note that the energy densities associated with the equatorial bonds are very small.

Of more relevance to this study, however, is the potential correlation between QTAIM parameters associated with the equatorial bonding and the U-O_{yl} vibrational frequencies. These data are presented in Figure 4. Here we have summed over the values of ρ_{BCP} for each uranium-ligand bond since it is the combined effect of the ligating species which leads to the variation in vibrational frequencies. Again, we find strong correlation (R^2 = 0.92, see Figure 4(a)) with the antisymmetric U-O_{yl} stretching mode. The correlation with the symmetric mode is slightly weaker (R^2 = 0.89, see Figure 4(a)), but still represents a strong relationship. This correlation demonstrates that the U-O_{yl} stretching modes, easily identifiable via IR or Raman spectroscopies, serve as a quantitative measure of equatorial bond covalency, as defined by the magnitude of the electron density at the QTAIM-derived BCP.

We next turn our attention to integrated properties of the electron density in order to better understand the contribution of the uranium centre to equatorial bond covalency in these systems. To do this, we make use of several QTAIM derived quantities: n_A, the electron population of atom A, obtained by integrating the electron density over the atomic basin Ω_A

and from which atomic charges can be deduced; λ_A, the localisation index, a measure of the number of electrons localised (i.e. not shared) on atom A; and δ_{AB}, the delocalisation index, a measure of the number of electrons shared between atoms A and B. The (de)localisation index is obtained via integration of the exchange-correlation component of the electron pair-density. We also define two further quantities: the uranyl electron population, n_{UO_2}, and the uranyl localisation index, λ_{UO_2}, defined as:

$$n_{UO_2} = n_U + \sum_i n_{O_i} \quad (1)$$

$$\lambda_{UO_2} = \lambda_U + \sum_i \left(\lambda_{O_i} + \delta_{UO_i} \right) + \delta_{OO} \quad (2)$$

For the isolated uranyl dication, n_{UO_2} and λ_{UO_2} are both equal to the total number of electrons in the system, 106. We can therefore use the corresponding values in our complexes to better understand the amount of electron density transferred to/from, and shared between, the uranyl unit and the equatorial ligands.

Table 6 presents the one-electron integrated QTAIM properties. Ligand populations and charges are not reported, since trends will, by definition, mirror those of q_{UO_2}. We find that there is an overall increase in electron population of the uranyl unit upon stronger equatorial complexation, leading to reduction in the formal +2 charge to a value as low as +0.88 upon complexation by hydroxide. There is a clear transfer of approximately 0.5 a.u. of electron density to the uranium centre upon complexation, however the electron population of the uranium atom remains approximately constant irrespective of the nature of the equatorial ligand. There is, in contrast, an increase of electronic charge on the O_{yl} atoms upon stronger equatorial complexation. This implies a charge transfer from ligand to uranyl oxygen,

inducing an increased ionic interaction between the positively charged uranium centre and the (increasingly) negatively charged oxygens.

While one-electron properties give us a gross description of charge transfer in these complexes, analysis of the two-electron properties, as given in Table 7, can provide greater insight into the variation in bonding character upon complexation. Focussing first on the localisation indices associated with individual atoms, we find a small decrease in λ_U along with a more pronounced increase in λ_O, similar to the trends found in atomic populations. This strengthens our previous assertion that equatorial complexation enhances the ionic character of the U-O_{yl} bond: the degree of electron localisation on the O_{yl} centres actually exceeds the degree of electron population increase.

In a previous study of a series of complexes of formally tetravalent actinides[61] we noted a strong correlation when comparing the quantity Z_{An}– λ_{An} (where Z is the atomic number) and the formal oxidation state. This relationship is again present: subtracting λ_U from the atomic number of uranium (Z = 92) furnishes a range of values between 5.88 and 6.12, in excellent agreement with the formal +VI oxidation state of uranium in these complexes.

Although the amount of charge transferred to the uranyl unit increases upon stronger equatorial complexation (see Table 6), the uranyl localisation index, λ_{UO_2}, remains largely unchanged. Since λ_{UO_2} also accounts for all electron delocalisation *within* the uranyl unit, this implies that the excess charge transferred by more strongly binding equatorial ligands is, in fact, delocalised between the uranium centre and equatorial ligands, i.e. this charge contributes to a covalent equatorial interaction. This necessitates a different origin for the increased electron population (and localisation) on the O_{yl} centres than that suggested by the one-electron data. The delocalisation index of the U-O_{yl} bond, which can be considered an alternative measure of bond covalency to that provided by ρ_{BCP}, is found to decrease upon

stronger equatorial complexation. The origin of the excess charge on the O_{yl} centres can therefore be understood as a localisation of charge previously delocalised in the U-O_{yl} bond. This provides the strongest evidence for our assertion that equatorial complexation enhances the ionic character of the U-O_{yl} bond: the elongation and weakening of the U-O_{yl} bond (as evidenced by the reduction in ν_{UO}) can now be understood as originating from the fact that this increased ionic interaction comes at the expense of U-O_{yl} bond covalency. This interpretation is, again, in keeping with the qualitative picture given by electron density differences, which show a clear depletion of charge in the U-O_{yl} bonding region along with an accumulation on the O_{yl} centres. The combined variation of n_{UO_2} and λ_{UO_2}, shown in the final column of Table 7, provides further evidence of the increase in equatorial covalent character. As the electron population of the uranyl unit increases, so the degree of electron localisation drops: equatorial complexation induces a covalent contribution to the bond from the uranium centre itself.

As was found with the U-O_{yl} ρ_{BCP} data, comparing the decrease in $\delta_{UO_{yl}}$ with the variation in U-O_{yl} stretch frequencies reveals a very strong correlation (R^2 = 1.00 and 0.99 for the antisymmetric and symmetric modes, respectively, see Figure S2 of ESI). Turning our attention to the more interesting potential relationship between U-O_{yl} vibrational frequencies and equatorial ligand covalency as measured by delocalisation index we again find strong correlation (R^2 = 0.94 and 0.93 for antisymmetric and symmetric modes, respectively, see Figure 5), further strengthening our finding that U-O_{yl} stretching modes serve as a quantitative measure of equatorial bond covalency.

We now consider the behaviour of another density based analytical tool, the electron localisation function[62,63] (ELF, denoted by $n(\mathbf{r})$). $n(\mathbf{r})$ is a scalar field, and its topology can be analysed in a similar way as $\rho(\mathbf{r})$[64]. Four types of stable critical points (CPs) can be

identified, with those denoted (3,-3) corresponding to local maxima and those denoted (3,-1) corresponding to saddle points. A strongly covalent interaction is characterised by a (3,-3) CP along the bond direction, unassociated with any nucleus, whereas the value of $n(\mathbf{r})$ at a (3,-1) CP defines a bifurcation point in $n(\mathbf{r})$. This bifurcation point represents a value for which an isosurface of $n(\mathbf{r})$ splits into two (or more) separate surfaces. These bifurcation points have previously been proposed as a measure of electron delocalisation between atomic basins[64–66].

Our topological analysis of $n(\mathbf{r})$ reveals no (3,-3) CPs associated with the U-O_{yl} bond in any complex considered here. However, all complexes exhibit (3,-1) CPs along the bond, the values of which are summarised in Table 8. These values represent the point at which $n(\mathbf{r})$ bifurcates into a set of separate surfaces each encompassing one of the uranyl atoms. The variation in these bifurcation points is very small and the values themselves do not correlate with any properties reported in this study. Analysis of the equatorial bonds reveals a similar picture: values of $n(\mathbf{r})$ at the (3,-1) CPs do not correlate with either the reported QTAIM parameters or physical properties of the ligands.

Inspecting the behaviour of $n(\mathbf{r})$ along the U-O_{yl} bond reveals some dependence on the strength of the equatorial coordination: approaching the (3,-1) CP from the uranyl centre (Figure 6a) reveals a small reduction in $n(\mathbf{r})$ broadly commensurate with the strength of the equatorial coordination. Approaching from the O_{yl} centre (Figure 6b) reveals the opposite behaviour, i.e. an increase in $n(\mathbf{r})$ for complexes exhibiting strong equatorial binding. While these observations may be indicative of variation in the U and O_{yl} contributions to the bond, a quantitative relationship is not obvious, particularly given the magnitude of the variation.

Since we have already demonstrated strong correlations between QTAIM parameters and the physical properties of the complexes considered here it would appear that, in these systems at

least, analysis of $n(\mathbf{r})$ provides little insight into the variation in axial bonding upon equatorial complexation.

Finally, we consider analysis of the reduced density gradient (RDG), defined as:

$$s(\mathbf{r}) = \frac{1}{2\left(3\pi^2\right)^{1/3}} \frac{\left|\nabla\rho(\mathbf{r})\right|}{\rho(\mathbf{r})^{4/3}}. \quad (3)$$

It has previously been demonstrated that in regions of both covalent and predominately noncovalent interactions, the reduced density gradient $s(\mathbf{r})$ assumes very small values. However, while $\rho(\mathbf{r})$ can be large in covalent bonding regions, it is small but non-zero in regions of largely noncovalent interaction, such as might be expected in the equatorial bonding regions of the complexes considered here. Plots of $s(\mathbf{r})$ against $\rho(\mathbf{r})$ exhibit spikes at low densities, indicating the presence of such interactions[67]. A more intuitive interpretation is obtained, however, by visualisation of the $s(\mathbf{r})$ isosurface, revealing the spatial regions in which these interactions are taking place. Since such interactions can be both attractive and repulsive, $s(\mathbf{r})$ isosurfaces are typically mapped with values of $\rho(\mathbf{r})\mathrm{sgn}\left(\lambda_2\right)$, where sgn($x$) is the signum function, returning -1 if $x < 0$ and 1 if $x > 0$, and λ_2 is the second largest eigenvalue of the Hessian of $\rho(\mathbf{r})$: λ_2 is typically negative (positive) for attractive (repulsive) interactions[67].

We present our analysis of the RDG in Figure 7. Here we present data for complexes involving weak (CO), intermediate (CN-) and strongly (F-) binding equatorial ligands. These are the same ligands for which we presented electron density differences in Figure 2. The isosurface of the carbonyl complex (Figure 7aii) reveals a region of spatially extended weak attraction girdling the uranium centre corresponding to the two spikes in Figure 7ai at negative values of $\rho(\mathbf{r})\mathrm{sgn}\left(\lambda_2\right)$. The spike at $\rho(\mathbf{r})\mathrm{sgn}\left(\lambda_2\right) \approx$ -0.04 a.u. defines a set of

circular attractive regions at the U-C bond centres. The spike occurring at positive $\rho(\mathbf{r})\mathrm{sgn}(\lambda_2)$ defines a weak repulsive annular area around each of these attractive regions. Turning our attention to the isocyano complex, a stronger and more directed attractive interaction is revealed, occurring at the U-N bond centres and characterised by a broader spike at a more negative value of $\rho(\mathbf{r})\mathrm{sgn}(\lambda_2) \approx$ -0.06 a.u. The spike at ~ -0.02 a.u. defines a set of weaker attractive regions between neighbouring cyanide ligands and, as before, the spike at ~ 0.02 a.u. defines a set of annular areas around each of the U-N bonding regions. Finally, the fluoro complex continues the trend: the region defining the U-F bonding interactions is again broader and occurs at a more negative value of $\rho(\mathbf{r})\mathrm{sgn}(\lambda_2) \approx$ -0.10 a.u., indicating a stronger interaction, whereas the extent of inter-ligand attractive region continues to reduce. The repulsive spike again defines a series of annular areas around the U-F bonding regions.

Summary and Conclusions

We have employed density functional theory (DFT) to investigate the effects of equatorial ligation on the U-O_{yl} bond of uranyl. The U-O_{yl} stretch vibrational frequencies are known to be sensitive probes of the equatorial coordination environment, and here we have demonstrated a strong correlation between these vibrational modes and the strength of equatorial bonding.

We have investigated the nature of this relationship through a series of analytical approaches, all of which are based on interrogation of the physically observable electron density. In order to obtain a qualitative understanding of the effects of equatorial ligation, we have produced plots of the electron density differences upon complexation. Visual analysis of these plots

provided an intuitive description of the bonding process: as equatorial bond strength increased, so density was transferred from the U-O_{yl} bonding region, implying a reduction in the covalent character of the bond. The charge was transferred partly onto the –yl oxygens, but also into the equatorial bonding region, indicating an increase in equatorial covalency.

In order to quantify the variation deduced from density difference plots, we turned to the quantum theory of atoms in molecules (QTAIM). This approach allowed us to investigate both topological and integrated properties of the electron density, and lent strong support to the qualitative description discussed above. Two key conclusions could be drawn from the QTAIM analysis: firstly, the redistribution of charge could not be fully understood by considering only one-electron integrated properties, i.e. atomic electron populations. The localisation and delocalisation indices, both two-electron properties, were required in order to elucidate this. The indices revealed a reduction in U-O_{yl} electron sharing, along with an increase in electron localisation on the O_{yl} centres, upon stronger equatorial complexation. This demonstrated a transition from covalent to more ionic bonding character, as well a contribution from the uranium centre to equatorial bond covalency. Secondly, and more importantly, QTAIM analysis demonstrated, for the first time, a strong correlation between U-O_{yl} vibrational frequencies and equatorial bond covalency. This correlation allows for the experimental probing of this covalency via UV-vis and Raman spectroscopies. We note that our conclusion of equatorial bond covalency in the fluoride complex is at odds with previous work[51], however we are confident that our analysis of electronic structure via one- and two-electron integrated properties, which supports both our topological analysis and our qualitative analysis based on density difference plots, support this conclusion.

We further interrogated the electron density by considering the behaviour of the electron localisation function (ELF). However, no correlation was found between properties of the ELF and bonding character/strength. Therefore, we turned our attention to analysis of the

reduced density gradient (RDG), which has previously been used to investigate regions of weak interaction as might be found in the equatorial bonds of these complexes. This analysis demonstrated a concentration and increased directionality of the bonding interaction as equatorial binding increased, as revealed in isosurface plots of the RDG. These plots bear a qualitative similarity to those of electron density accumulation in the equatorial bonding region, and support the findings of our energetic and QTAIM analyses. This reaffirms the utility of the density difference plots as a simple visual depiction of bonding character which can be supported by quantitative analysis of the electron density.

In summary, we have demonstrated that a deep understanding of bonding can be gleaned from combined analyses of the electron density. Furthermore, we have correlated quantitative data from these analyses with experimentally accessible measures. Strong correlation suggests that this approach will be of use when applied to more complex systems and could be used predictively in order to better understand environments in which experimental probes are impractical: in particular, we envision application in developing a better understanding of actinide complexation in environments in which spent nuclear fuel is stored. This area forms the focus of our ongoing research.

Supporting Information Available: density difference plots for all complexes considered, correlation data between vibrational and topological properties, TPSSh/TZVP optimised structural parameters and total energies.

Acknowledgements

We would like to thank the EPSRC for the award of a career acceleration fellowship (grant EP/J002208/1), the High End Computing facility at Lancaster University for access to HPC resources and the National Service for Computational Chemistry Software (NSCCS) for

access to the Slater HPC facility. We also thank Prof. Nik Kaltsoyannis and Dr. Michael Patzschke for helpful discussions.

References

(1) Wang, D.; van Gunsteren, W. F.; Chai, Z. *Chem. Soc. Rev.* **2012**, *41*, 5836–5865.

(2) Kaltsoyannis, N. *Inorg. Chem.* **2013**, *52*, 3407–3413.

(3) Dam, H. H.; Reinhoudt, D. N.; Verboom, W. *Chem. Soc. Rev.* **2007**, *36*, 367–377.

(4) Lewis, F.; Hudson, M.; Harwood, L. *Synlett* **2011**, *2011*, 2609–2632.

(5) Allen, P. G.; Bucher, J. J.; Shuh, D. K.; Edelstein, N. M.; Reich, T. *Inorg. Chem.* **1997**, *36*, 4676–4683.

(6) Wahlgren, U.; Moll, H.; Grenthe, I.; Schimmelpfennig, B.; Maron, L.; Vallet, V.; Gropen, O. *J. Phys. Chem. A* **1999**, *103*, 8257–8264.

(7) Rowland, C. E.; Kanatzidis, M. G.; Soderholm, L. *Inorg. Chem.* **2012**, *51*, 11798–11804.

(8) Berthet, J.-C.; Thuéry, P.; Ephritikhine, M. *Chem. Commun.* **2007**, 604–606.

(9) Vallet, V.; Wahlgren, U.; Schimmelpfennig, B.; Moll, H.; Szabó, Z.; Grenthe, I. *Inorg. Chem.* **2001**, *40*, 3516–3525.

(10) Straka, M.; Dyall, K. G.; Pyykkö, P. *Theor. Chem. Accounts Theory, Comput. Model. (Theoretica Chim. Acta)* **2001**, *106*, 393–403.

(11) Spencer, S.; Gagliardi, L.; Handy, N. C.; Ioannou, A. G.; Skylaris, C.; Willetts, A.; Simper, A. M. *J. Phys. Chem. A* **1999**, *103*, 1831–1837.

(12) Hay, P. J.; Martin, R. L.; Schreckenbach, G. *J. Phys. Chem. A* **2000**, *104*, 6259–6270.

(13) Ingram, K. I. M.; Häller, L. J. L.; Kaltsoyannis, N. *Dalton Trans.* **2006**, *2*, 2403–2414.

(14) Austin, J. P.; Sundararajan, M.; Vincent, M. A.; Hillier, I. H. *Dalt. Trans.* **2009**, 5902–5909.

(15) Sonnenberg, J. L.; Hay, P. J.; Martin, R. L.; Bursten, B. E. *Inorg. Chem.* **2005**, *44*, 2255–2262.

(16) Iché-Tarrat, N.; Barros, N.; Marsden, C. J.; Maron, L. *Chem. - A Eur. J.* **2008**, *14*, 2093–2099.

(17) Fillaux, C.; Guillaumont, D.; Berthet, J.-C.; Copping, R.; Shuh, D. K.; Tyliszczak, T.; Den Auwer, C. *Phys. Chem. Chem. Phys.* **2010**, *12*, 14253–14262.

(18) Tsushima, S. *Dalton Trans.* **2011**, *40*, 6732–6737.

(19) Ahlrichs, R.; Bär, M.; Häser, M.; Horn, H.; Kölmel, C. *Chem. Phys. Lett.* **1989**, *162*, 165–169.

(20) Weigend, F.; Ahlrichs, R. *Phys. Chem. Chem. Phys.* **2005**, *7*, 3297–3305.

(21) Küchle, W.; Dolg, M.; Stoll, H.; Preuss, H. *J. Chem. Phys.* **1994**, *100*, 7535.

(22) Pantazis, D. A.; Neese, F. *J. Chem. Theory Comput.* **2011**, *7*, 677–684.

(23) Douglas, M.; Kroll, N. *Ann. Phys. (N. Y).* **1974**, *155*, 89–155.

(24) Hess, B. *Phys. Rev. A* **1986**, *33*, 3742–3748.

(25) Tao, J.; Perdew, J.; Staroverov, V.; Scuseria, G. *Phys. Rev. Lett.* **2003**, *91*, 146401.

(26) Staroverov, V. N.; Scuseria, G. E.; Tao, J.; Perdew, J. P. *J. Chem. Phys.* **2003**, *119* , 12129.

(27) Wåhlin, P.; Danilo, C.; Vallet, V.; Réal, F.; Flament, J.-P.; Wahlgren, U. *J. Chem. Theory Comput.* **2008**, *4*, 569–577.

(28) Prodan, I.; Scuseria, G.; Martin, R. *Phys. Rev. B* **2006**, *73*, 045104.

(29) Kerridge, A.; Kaltsoyannis, N. *Chemistry* **2011**, *17*, 5060–5067.

(30) Perdew, J.; Burke, K.; Ernzerhof, M. *Phys. Rev. Lett.* **1996**, *77*, 3865–3868.

(31) Becke, A. D. *J. Chem. Phys.* **1993**, *98*, 5648.

(32) Stephens, P.; Devlin, F.; Chabalowski, C.; Frisch, M. *J. Phys. Chem.* **1994**, *98*, 11623–11627.

(33) Klamt, A.; Schüürmann, G. *Perkins Trans.* **1993**, *2*, 799–805.

(34) Keith, T. A. *AIMAll (Version 14.11.23), TK Gristmill Software, Overl. Park KS, USA* **2014**.

(35) Lu, T.; Chen, F. *J. Comput. Chem.* **2012**, *33*, 580–592.

(36) Glendening, E. D.; Badenhoop, J. K.; Reed, E. A.; Carpenter, J. E.; Bohmann, J. A.; Morales, C. M.; Landis, C. R.; Weinhold, F. *NBO 6.0 , Theor. Chem. Institute, Univ. Wisconsin, Madison, WI* **2013**.

(37) Görller-Walrand, C.; Houwer, S. De; Fluyt, L.; Binnemans, K. *Phys. Chem. Chem. Phys.* **2004**, *6*, 3292–3298.

(38) Serezhkin, V. . In *Structural Chemistry of Inorganic Actinide Compounds*; Krivovichev, S. V., Burns, P. C., Tananaev, I. G., Eds.; Elsevier B.V.: Amsterdam, 2007.

(39) Lychev, A. A.; Mashirov, L. G.; Smolin, Y. I.; Shepelev, Y. . *Sov. Radiochem.* **1986**, *28*, 622–625.

(40) Ricks, A. M.; Gagliardi, L.; Duncan, M. a. *J. Am. Chem. Soc.* **2010**, *132*, 15905–15907.

(41) Clavaguéra-Sarrio, C.; Brenner, V.; Hoyau, S.; Marsden, C. J.; Millie, P.; Dognon, J. P. *J. Phys. Chem. B* **2003**, *107*, 3051–3060.

(42) Schreckenbach, G.; Hay, P. J.; Martin, R. L. *Inorg. Chem.* **1998**, *37*, 4442–4451.

(43) Tsushima, S.; Reich, T. *Chem. Phys. Lett.* **2001**, *347* (October), 127–132.

(44) Odoh, S. O.; Walker, S. M.; Meier, M.; Stetefeld, J.; Schreckenbach, G. *Inorg. Chem.* **2011**, *50*, 3141–3152.

(45) Ruipérez, F.; Wahlgren, U. *J. Phys. Chem. A* **2010**, *114*, 3615–3621.

(46) Hashem, E.; Platts, J. A.; Lorusso, G.; Evangelisti, M.; Schulzke, C.; Baker, R. J. *Inorg. Chem.* **2014**, *53*, 8624–8637.

(47) Clark, D. L.; Conradson, S. D.; Donohoe, R. J.; Keogh, D. W.; Morris, D. E.; Palmer, P. D.; Rogers, R. D.; Tait, C. D. **1999**, *38*, 1456–1466.

(48) Bullock, J. I. *J. Chem. Soc. A* **1969**, 781–784.

(49) Toth, L. M.; Begun, G. M. *J. Phys. Chem.* **1981**, *85*, 547–549.

(50) Nguyen-Trung, C.; Palmer, D. A.; Begun, G. M.; Peiffert, C.; Mesmer, R. E. *J. Solution Chem.* **2000**, *29*, 101–129.

(51) Vallet, V.; Wahlgren, U.; Grenthe, I. *J. Phys. Chem. A* **2012**, *116*, 12373–12380.

(52) Hong, G.; Schautz, F.; Dolg, M. *J. Am. Chem. Soc.* **1999**, *121*, 1502–1512.

(53) Gagliardi, L.; Roos, B. *Nature* **2005**, *433* (February), 848–851.

(54) Pierloot, K.; van Besien, E. *J. Chem. Phys.* **2005**, *123*, 204309.

(55) Kerridge, A.; Coates, R.; Kaltsoyannis, N. *J. Phys. Chem. A* **2009**, *113*, 2896–2905.

(56) Kerridge, A.; Kaltsoyannis, N. *J. Phys. Chem. A* **2009**, *113*, 8737–8745.

(57) Clark, A. E.; Sonnenberg, J. L.; Hay, P. J.; Martin, R. L. *J. Chem. Phys.* **2004**, *121*, 2563–2570.

(58) Tassell, M. J.; Kaltsoyannis, N. *Dalt. Trans.* **2010**, *39*, 6576–6588.

(59) Kirker, I.; Kaltsoyannis, N. *Dalton Trans.* **2011**, *40*, 124–131.

(60) Kerridge, A. *Dalton Trans.* **2013**, *42*, 16428–16436.

(61) Kerridge, A. *RSC Adv.* **2014**, *4*, 12078–12086.

(62) Becke, A. D.; Edgecombe, K. E. *J. Chem. Phys.* **1990**, *92*, 5397.

(63) Silvi, B.; Savin, A. *Nature* **1994**, 371, 683.

(64) Savin, A.; Silvi, B.; Colonna, F. *Can. J. Chem.* **1996**, *74*, 1088–1096.

(65) Savin, A.; Nesper, R.; Wengert, S.; Fassler, T. E. *Angew. Chemie Int. Ed.* **1997**, *36*, 1808–1832.

(66) Alikhani, M. E.; Fuster, F.; Silvi, B. *Struct. Chem.* **2005**, *16*, 203–210.

(67) Johnson, E. R.; Keinan, S.; Mori-Sánchez, P.; Contreras-García, J.; Cohen, A. J.; Yang, W. *J. Am. Chem. Soc.* **2010**, *132*, 6498–6506.

Figures

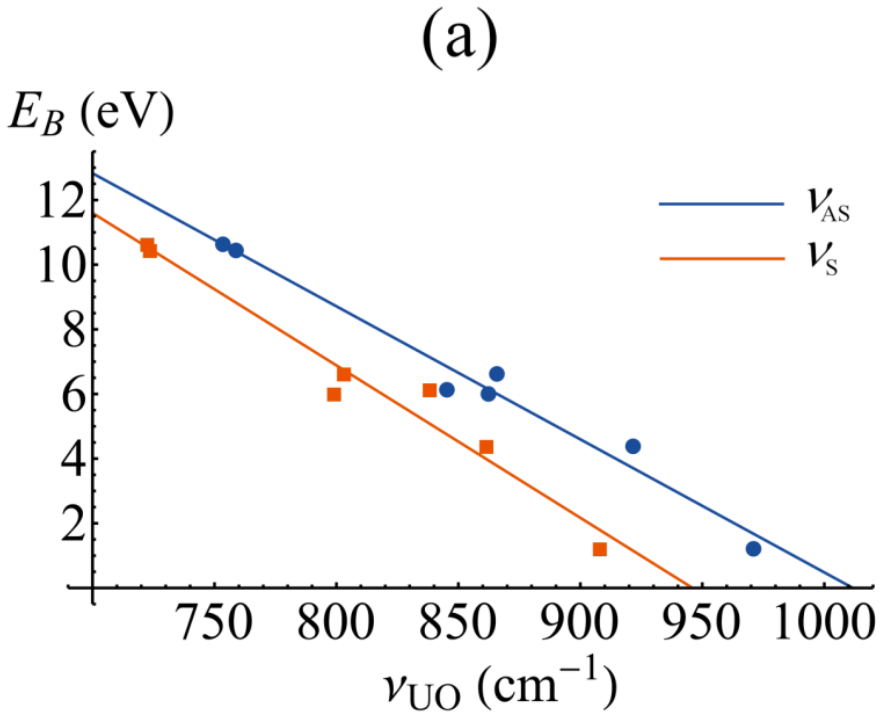
(a)
E_B (eV)
12
10
8
6
4
2
750
800
850
900
950
1000
ν_{UO} (cm^{-1})
ν_{AS}
ν_S

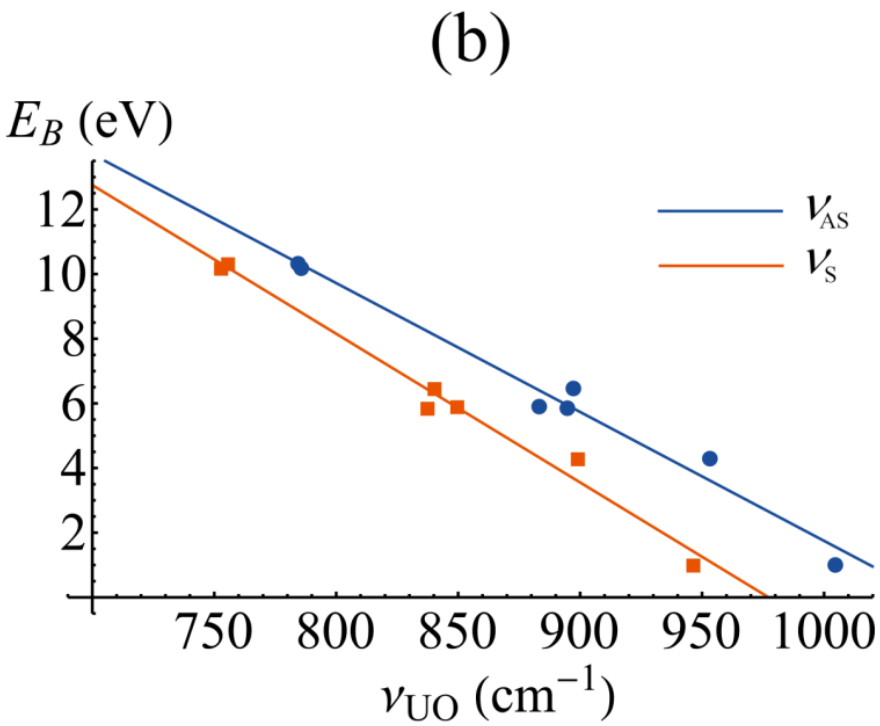
(b)
E_B (eV)
12
10
8
6
4
2
750
800
850
900
950
1000
ν_{UO} (cm^{-1})
ν_{AS}
ν_S

Figure 1. Linear fitting of calculated U-O_{yl} vibrational frequencies to binding energies. a) TPSS data: R^2 = 0.98 and 0.96 for antisymmetric and symmetric stretch modes, respectively. b) TPSSh data: R^2 = 0.98 for both antisymmetric and symmetric stretch modes, respectively.

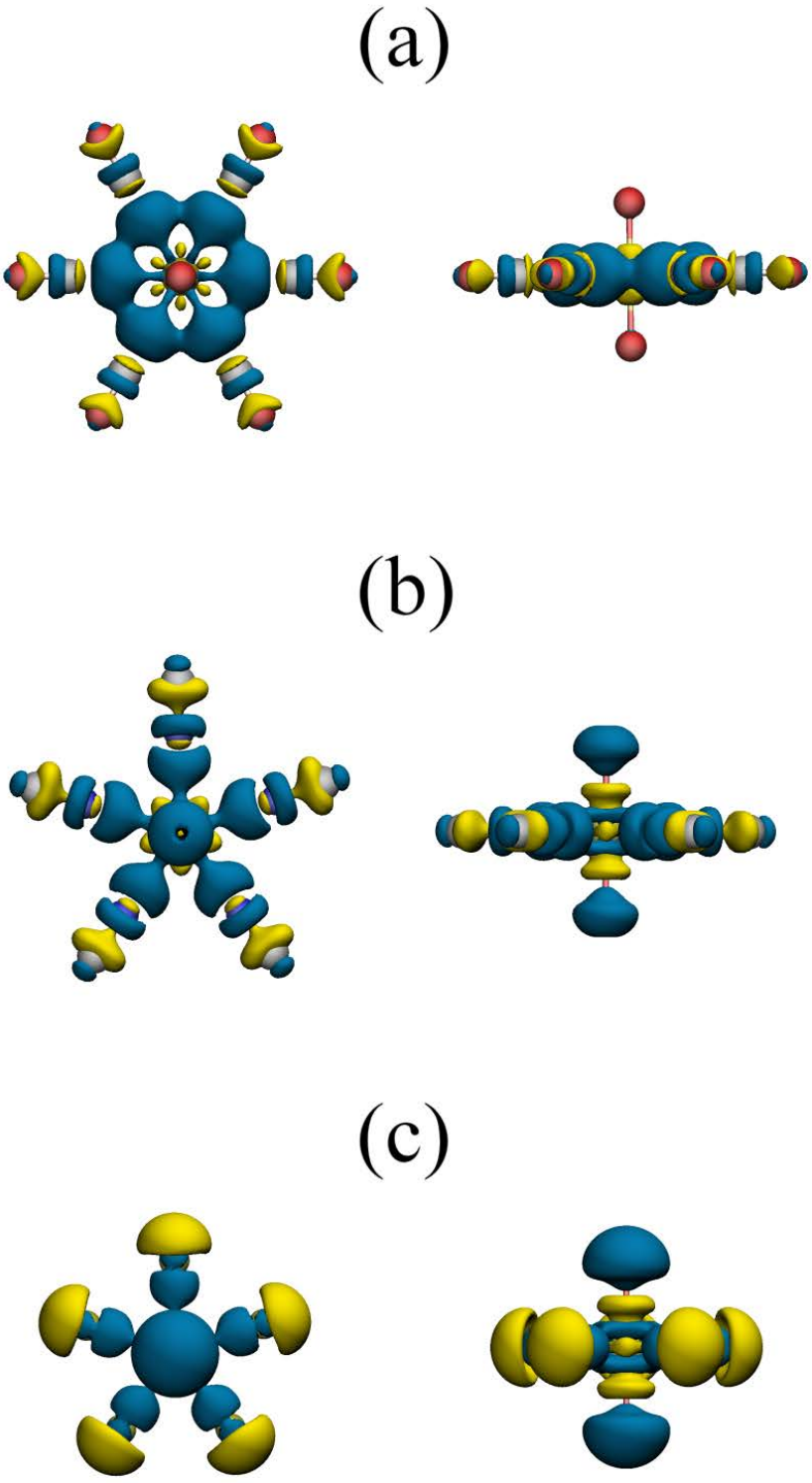

Figure 2. Density difference plots of the a) carbonyl, b) isocyano and c) fluoro complexes of uranyl, calculated by subtracting the TPSSh-calculated electron densities of the uranyl and

ligand fragments from that of the full complexes . Blue regions indicates areas of electronic charge accumulation and yellow regions charge depletion. Molecular structures drawn to same scale. All isosurfaces rendered at a value of 0.005 a.u.

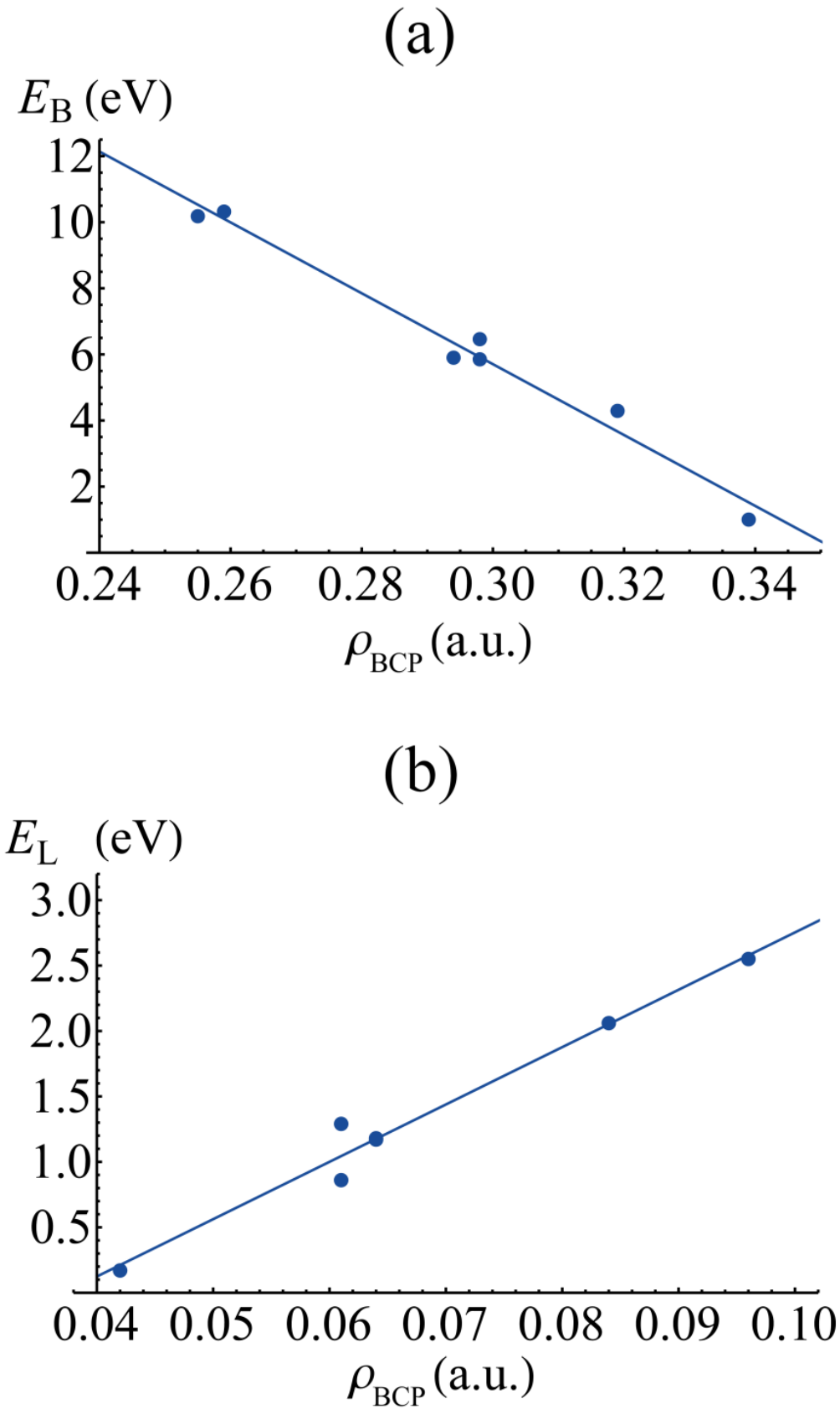

Figure 3. Correlation of a) total binding energy (E_B) with U-O_{yl} ρ_{BCP} values and b) per ligand binding energy (E_B) with U-L ρ_{BCP} values.

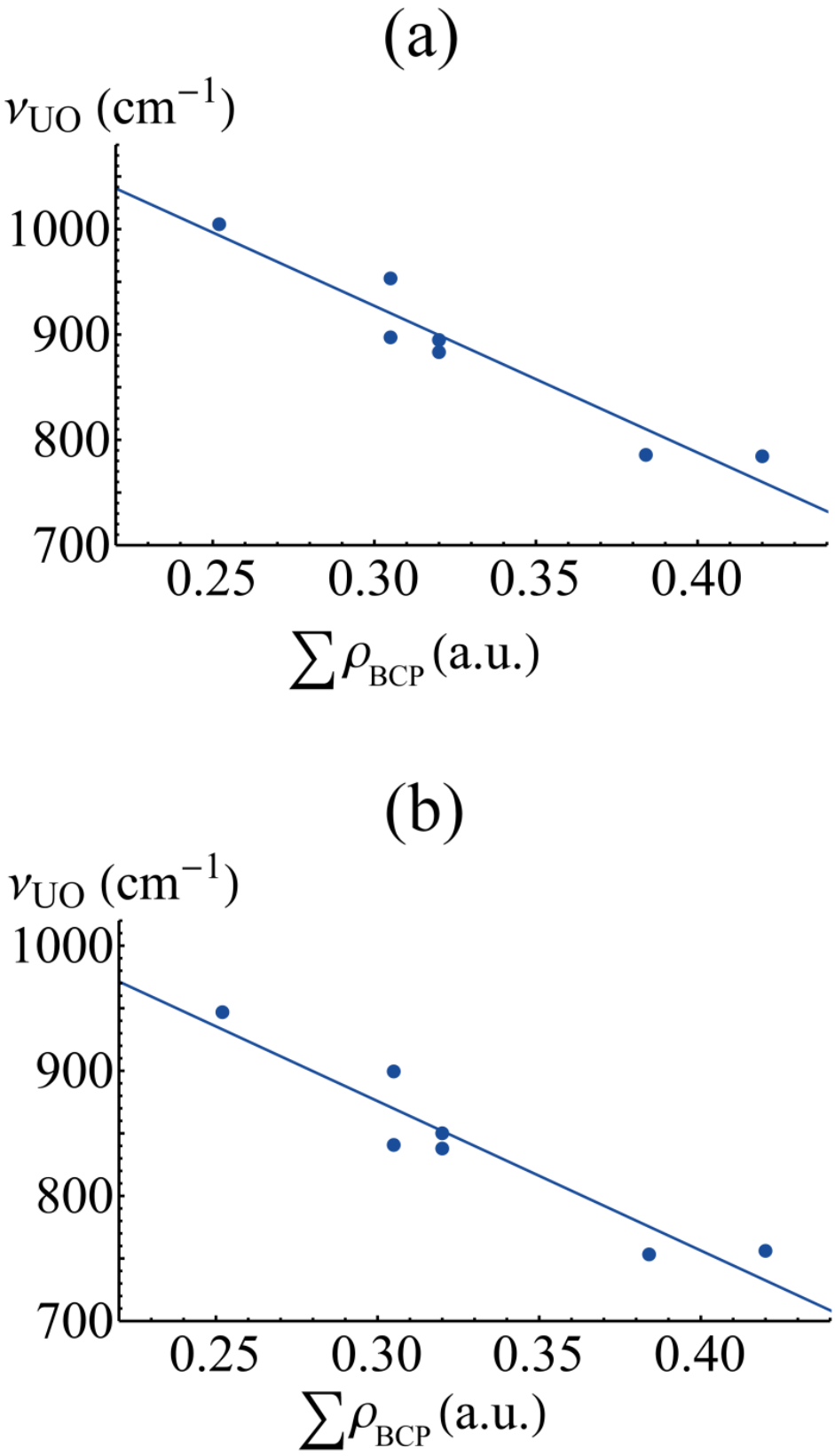

Figure 4. Correlation of a) U-O_{yl} antisymmetric and b) symmetric stretch vibrational frequencies with the sum of electron densities at the equatorial ligand BCPs.

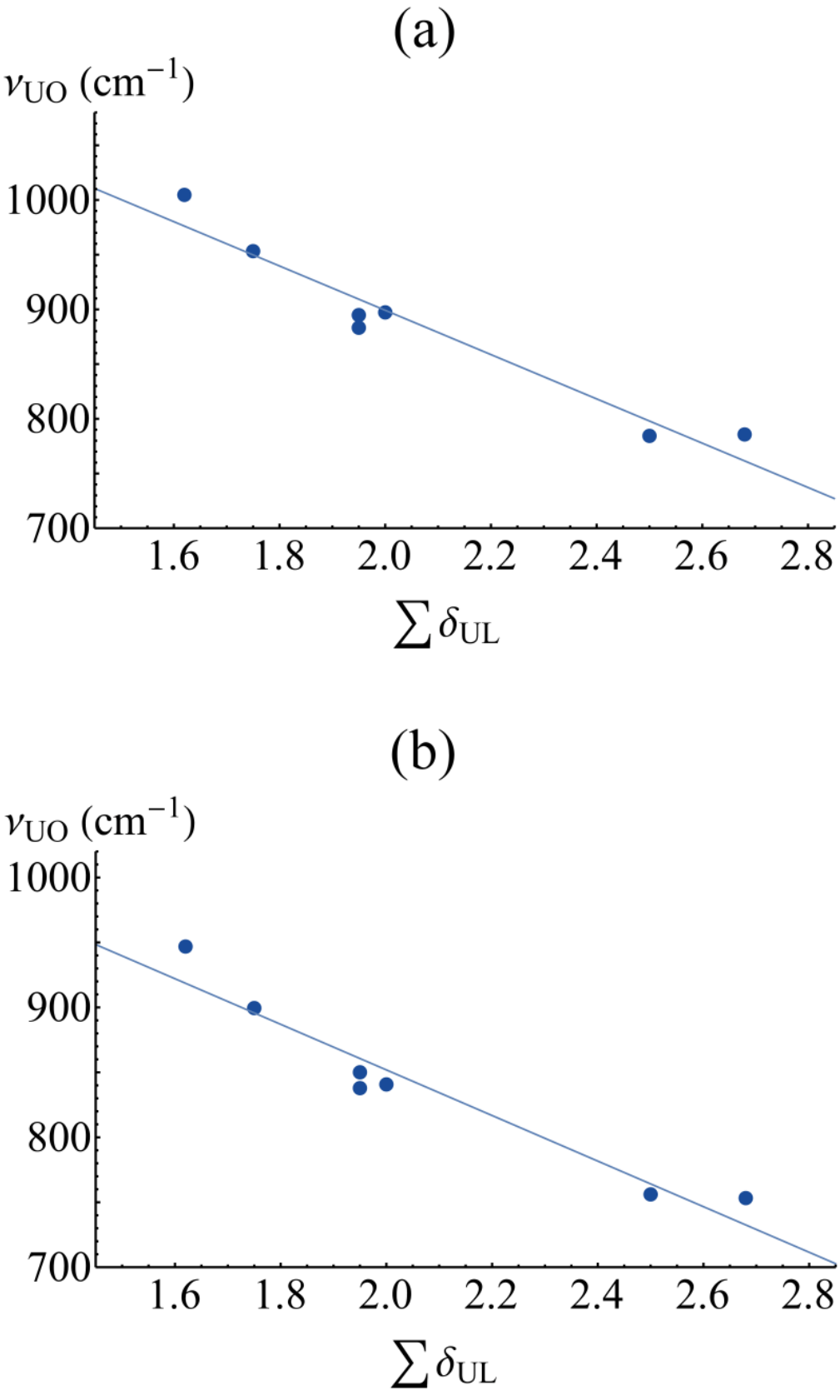

Figure 5. Correlation of a) U-O_{yl} antisymmetric and b) symmetric stretch vibrational frequencies with the sum of uranium-ligand delocalisation indices.

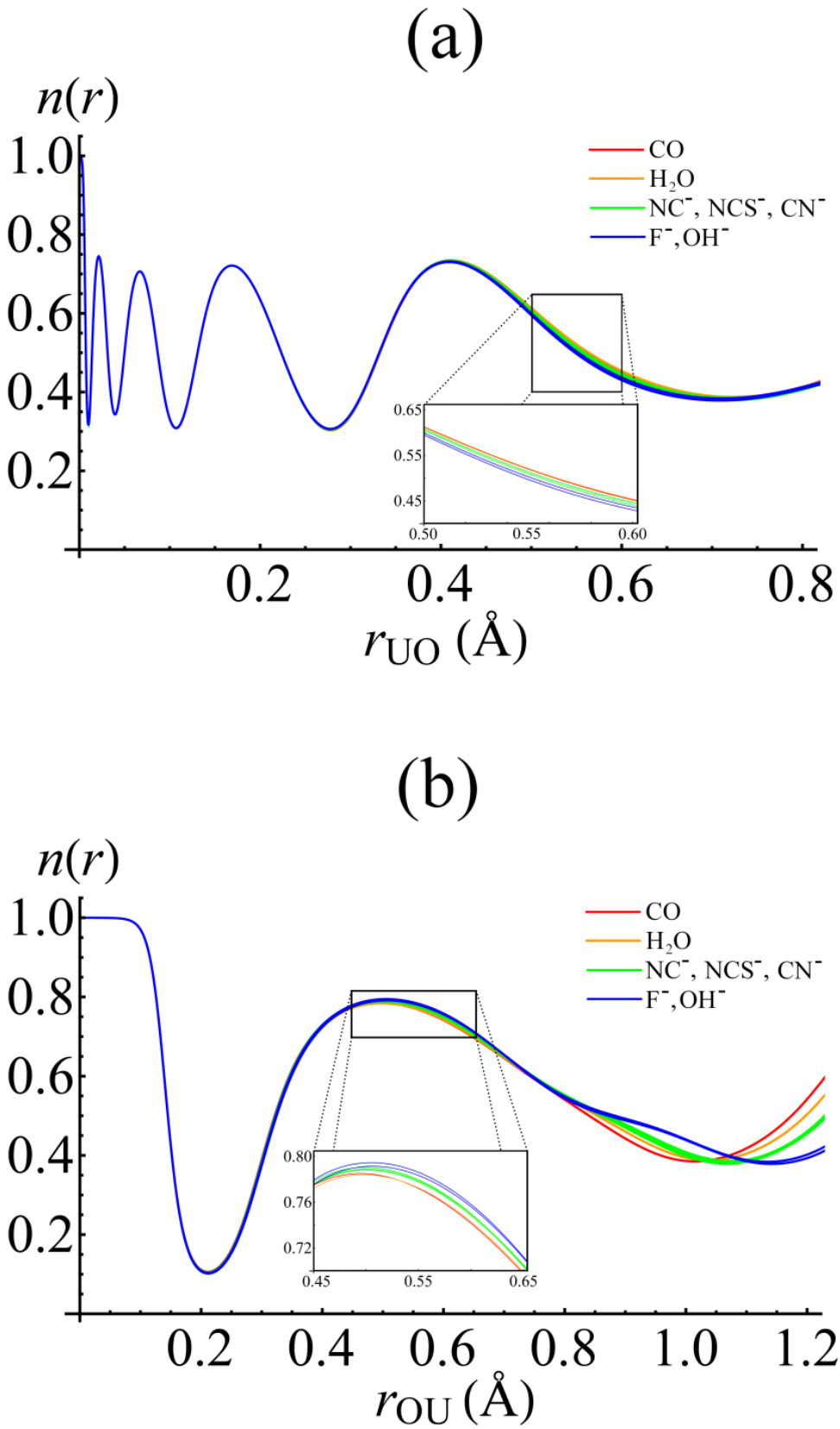

Figure 6. Behaviour of the electron localisation function, $n(\mathbf{r})$, along the U-O_{yl} bond. (a) $n(\mathbf{r})$ between the uranium centre and (3,-1) CP; (b) $n(\mathbf{r})$ between the oxygen centre and the (3,-1) CP.

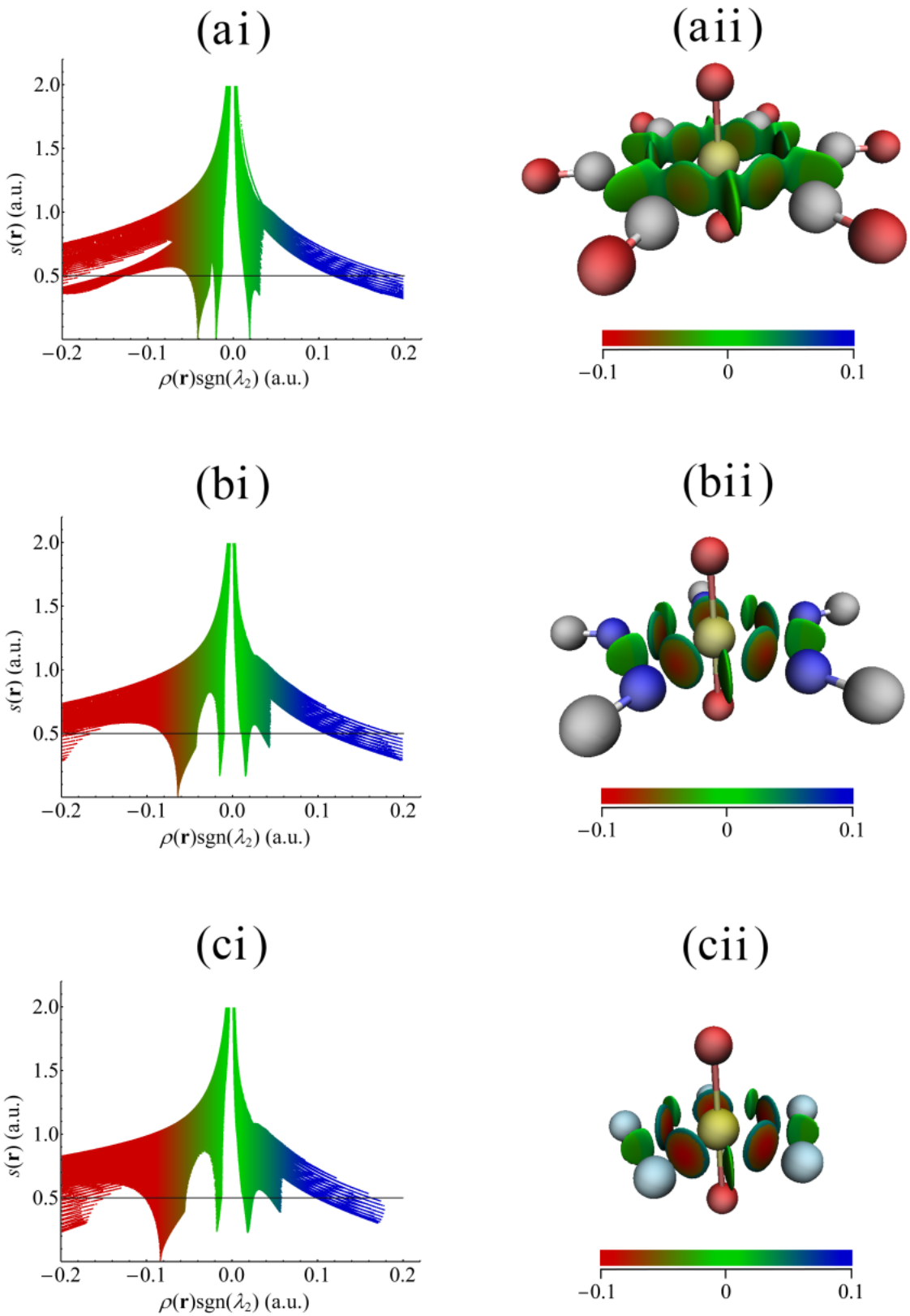

Figure 7. Analysis of the reduced density gradient (RDG) for a) $[UO_2(CO)_6]^{2+}$ b) $[UO_2(NC)_5]^{3-}$ and c) $[UO_2F_5]^{3-}$. Colour mapping is identical in all plots. Isosurfaces are rendered at $s(\mathbf{r})$ = 0.5 a.u., corresponding to the horizontal lines in the left hand panes.

Tables

Table 1. DFT-calculated total binding energies of carbonyl, cyano, isocyano and fluoro complexes as a function of equatorial coordination number. All values are given in eV. Italicised entries indicate most stable complexes.

Ligand	Coordination number					
	4		5		6	
	TPSS	TPSSh	TPSS	TPSSh	TPSS	TPSSh
CO	*0.88*	*0.73*	0.83	0.70	1.21	1.00
CN-	5.72	5.54	*6.62*	*6.46*	6.49	6.26
NC-	5.63	5.47	*6.00*	*5.85*	5.21	5.00
F-	10.32	10.03	*10.63*	*10.32*	9.78	9.26

Table 2. DFT-calculated structural parameters of energetically stable uranyl complexes considered in the first part of this study, along with comparisons to experimental data. [a] solid state XRD (ref [8]); [b] solid state XRD (ref [7]); [c] solution EXAFS (ref [6]); [d] solution EXAFS (ref [5]); [e] solid state XRD (ref [47]); [f] solution EXAFS (ref [9]). [†] Mean bond lengths.

Ligand	CN	symmetry	r_{UO} (Å)					r_{UL} (Å)				
			TPPS	PBE	TPSSh	B3LYP	Exp.	TPPS	PBE	TPSSh	B3LYP	Exp.
CO	6	D_{6h}	1.752	1.755	1.736	1.733	-	2.710	2.705	2.717	2.782	-
CN^-	5	D_{5h}	1.804	1.807	1.786	1.784	1.773[†a]	2.568	2.562	2.568	2.591	2.567[†a]
NC^-	5	D_{5h}	1.805	1.806	1.787	1.784	-	2.463	2.468	2.462	2.485	-
NCS^-	5	D_{5h}	1.814	1.815	1.792	1.788	1.762[†b]	2.440	2.445	2.439	2.467	2.446[†b]
OH_2	5	C_2	1.777	1.779	1.761	1.759	1.78[c], 1.760[d]	2.427[†]	2.434[†]	2.424[†]	2.442[†]	2.41[c], 2.41[d]
OH^-	4	D_{2d}	1.869	1.871	1.849	1.846	1.82[c], 1.82[†e]	2.255	2.258	2.250	2.264	2.24[c], 2.26[†e]
F^-	5	D_{5h}	1.866	1.865	1.844	1.838	1.80[f]	2.258	2.267	2.255	2.274	2.26[f]
MAD			0.041	0.042	0.025	0.022		0.006	0.009	0.005	0.021	

Table 3. DFT-calculated U- O_{yl} stretch vibrational frequencies of energetically stable uranyl complexes considered in this study.

Ligand	CN	ν_S (cm^{-1})				ν_{AS} (cm^{-1})			
		TPSS	PBE	TPSSh	B3LYP	TPSS	PBE	TPSSh	B3LYP
CO	6	908	902	947	958	971	965	1005	1006
CN^-	5	804	798	841	848	866	861	897	902
NC^-	5	799	797	838	848	862	861	895	902
NCS^-	5	839	774	850	844	845	847	883	891
OH_2	5	862	859	899	908	922	920	953	960
OH^-	4	724	720	753	760	759	756	786	786
F^-	5	723	720	756	768	753	753	784	795

Table 4. DFT-calculated total (E_B) and per ligand (E_L) binding energies of energetically stable uranyl complexes. $E_L = E_B/CN$ gives the binding energy per ligand.

Ligand	CN	TPSS		PBE		TPSSh		B3LYP	
		E_B (eV)	E_L (eV)	E_B (eV)	E_L (eV)	E_B (eV)	E_L (eV)	E_B (eV)	E_L (eV)
CO	6	1.21	0.20	1.51	0.25	1.00	0.17	0.40	0.07
OH_2	5	4.38	0.88	4.68	0.94	4.29	0.86	4.19	0.84
NC^-	5	6.00	1.20	6.55	1.31	5.85	1.17	5.81	1.16
NCS^-	5	6.13	1.23	6.65	1.33	5.90	1.18	5.79	1.16
CN^-	5	6.62	1.32	7.24	1.45	6.46	1.29	6.32	1.26
F^-	5	10.63	2.13	10.88	2.18	10.32	2.06	9.97	1.99
OH^-	4	10.44	2.61	10.15	2.54	10.18	2.55	10.25	2.56

Table 5. Topological parameters associated with all uranium bonds, obtained via QTAIM analysis of TPSSh-derived densities. ρ_{BCP} is the magnitude of the electron density at the bond critical point (BCP), $\nabla^2\rho_{BCP}$ it's Laplacian, and H is energy density at the BCP

Complex	U-O_{yl}			U-X/U-L		
	ρ_{BCP} (a.u.)	$\nabla^2\rho_{BCP}$ (a.u.)	H (a.u)	ρ_{BCP} (a.u.)	$\nabla^2\rho_{BCP}$ (a.u.)	H (a.u)
$[UO_2]^{2+}$	0.364	0.309	-0.393	-	-	-
$[UO_2(CO)_6]^{2+}$	0.339	0.300	-0.344	0.042	0.105	-0.003
$[UO_2(H_2O)_5]^{2+}$	0.319	0.300	-0.307	0.061	0.222	-0.006
$[UO_2(NC)_5]^{3-}$	0.298	0.305	-0.270	0.064	0.186	-0.008
$[UO_2(NCS)_5]^{3-}$	0.294	0.301	-0.263	0.064	0.207	-0.007
$[UO_2(CN)_5]^{3-}$	0.298	0.311	-0.270	0.061	0.120	-0.009
$[UO_2(F)_5]^{3-}$	0.259	0.317	-0.204	0.084	0.328	-0.014
$[UO_2(OH)_4]^{2-}$	0.255	0.328	-0.199	0.096	0.293	-0.023

Table 6. One-electron integrated QTAIM parameters of uranyl and complexing ligands, obtained via analysis of TPSSh-derived densities. *n* and *q* are electronic populations and overall charges, respectively.

Complex	n_U (q_U)	$n_{O_{yl}}$ ($q_{O_{yl}}$)	n_{UO_2} (q_{UO_2})
$[UO_2]^{2+}$	88.57 (+3.43)	8.72 (-0.72)	106 (+2)
$[UO_2(CO)_6]^{2+}$	89.07 (+2.93)	8.77 (-0.77)	106.61 (+1.39)
$[UO_2(H_2O)_5]^{2+}$	88.89 (+3.11)	8.85 (-0.85)	106.59 (+1.59)
$[UO_2(NC)_5]^{3-}$	88.94 (+3.06)	8.93 (-0.93)	106.80 (+1.20)
$[UO_2(NCS)_5]^{3-}$	88.96 (+3.04)	8.94 (-0.94)	106.84 (+1.14)
$[UO_2(CN)_5]^{3-}$	89.09 (+2.91)	8.93 (-0.93)	106.95 (+1.05)
$[UO_2(F)_5]^{3-}$	88.84 (+3.16)	9.05 (-1.05)	106.94 (+1.06)
$[UO_2(OH)_4]^{2-}$	89.00 (+3.00)	9.06 (-1.06)	107.12 (+0.88)

Table 7. Two-electron integrated QTAIM parameters of uranyl and complexing ligands, obtained via analysis of TPSSh-derived densities. †delocalisation indices between uranium and coordinating species of the ligand, averaged over all ligands.

Complex	λ_{U}	$\lambda_{O_{yl}}$	λ_{UO_2}	$\delta_{UO_{yl}}$	$\delta_{OO_{yl}}$	δ_{UL} †	$(n-\lambda)_{UO_2}$
$[UO_2]^{2+}$	86.38	7.56	106	2.19	0.11	-	0.00
$[UO_2(CO)_6]^{2+}$	86.12	7.59	105.33	2.06	0.11	0.27	+1.08
$[UO_2(H_2O)_5]^{2+}$	86.02	7.73	105.52	1.97	0.10	0.35	+1.07
$[UO_2(NC)_5]^{3-}$	86.00	7.82	105.49	1.88	0.09	0.39	+1.31
$[UO_2(NCS)_5]^{3-}$	85.97	7.83	105.44	1.86	0.09	0.39	+1.40
$[UO_2(CN)_5]^{3-}$	86.07	7.80	105.52	1.88	0.09	0.40	+1.43
$[UO_2(F)_5]^{3-}$	85.88	8.02	105.42	1.71	0.08	0.50	+1.52
$[UO_2(OH)_4]^{2-}$	85.92	8.04	105.47	1.70	0.07	0.67	+1.65

Table 8: (3,-1) critical points of the electron localisation function $n(\mathbf{r})$ associated with axial and equatorial bonding to the uranium centre in all complexes studied.

Complex	$n^{c}_{UO_{yl}}$	n^{c}_{UL}
$[UO_2]^{2+}$	0.378	-
$[UO_2(CO)_6]^{2+}$	0.385	0.168
$[UO_2(H_2O)_5]^{2+}$	0.388	0.160
$[UO_2(NC)_5]^{3-}$	0.384	0.210
$[UO_2(NCS)_5]^{3-}$	0.386	0.190
$[UO_2(CN)_5]^{3-}$	0.379	0.274
$[UO_2(F)_5]^{3-}$	0.384	0.185
$[UO_2(OH)_4]^{2-}$	0.379	0.258

For Table of Contents Only

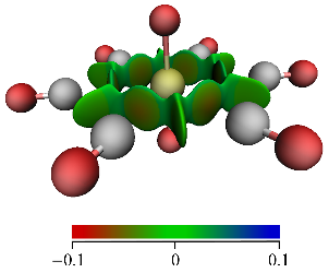

Simulation of a series of uranyl complexes reveals strong correlations between the degree of equatorial covalency and the nature and strength of axial U-O bonding. Quantitative analyses of the electron density agree with qualitative pictorial density difference representations and show that the axial U-O stretch vibrational modes may be used as a quantitative experimental probe of equatorial covalency.